Acta Cryst. (1997). A**53**, 187–198

A Topological Analysis of Charge Densities in Diamond, Silicon and Germanium Crystals

YU. A. ABRAMOV*† AND F. P. OKAMURA

National Institute for Research in Inorganic Materials, Namiki 1-1, Tsukuba, Ibaraki 305, Japan. E-mail: yuri@xraysg.umsl.edu

(Received 10 June 1996; accepted 23 October 1996)

Abstract

The Hansen–Coppens multipole model of charge density has been fitted to highly accurate published experimental and theoretical structure factors for diamond, silicon and germanium crystals. Analysis of both model experimental and theoretical charge densities using the resulting model parameters was performed in terms of Bader's topological theory. The general topology of the charge density appeared to be identical for all crystals, containing the four possible types of critical points of rank three, and no non-nuclear attractors between neighboring atoms were found within achieved accuracy. Theoretical and experimental values of charge density and its Laplacian show quantitative and semiquantitative agreement, respectively, at the critical points of model charge densities. For Ge crystals, such agreement is worse at the ring critical point. These results suggest the possibility of semiquantitative (within 10–30%) study of the topological characteristics of highly accurate X-ray charge densities of crystals displaying shared interatomic interactions. Comparative topological analysis of the chemical bond in this series of crystals is discussed in terms of the quantum topological theory.

1. Introduction

Bader's quantum-topological analysis of the charge density (Bader, 1990; Tsirelson & Ozerov, 1996) suggests a model of the chemical bond that takes advantage of the interrelation between the charge-density distribution, $\rho(\mathbf{r})$, the local energy and the chemical bond. This method does not rely on a reference density for analyzing the chemical bond and thus is free of some of the uncertainties of the deformation-electron-density approach for electron-rich atoms (*e.g.* Savariault & Lehmann, 1980; Dunitz & Seiler, 1983; Dunitz, Schweizer & Seiler, 1983). The topological approach was initially mainly applied to the analysis of theoretical charge densities. The field of its application to experimental (X-ray diffraction) charge densities is rapidly developing now (*e.g.* Kapphahn, Tsirelson & Ozerov, 1988; Craven & Stewart, 1990; Gatti, Bianchi, Destro & Merati, 1992; Destro & Merati, 1995; Iversen, Larsen, Souhassou & Takata, 1995; Tsirelson & Ozerov, 1996) owing to the possibility of analytically representing experimental ρ by various multipole techniques (Hirshfeld, 1971; Stewart, 1976; Hansen & Coppens, 1978), allowing analytical evaluation of the Laplacian, $\nabla^2\rho$, and gradient vector field of ρ. Although it seems that there is no fundamental restriction on the applicability of topological analysis to experimental ρ (Tsirelson, 1996), the numerical results in this case are affected by the thermal atomic motions in crystals (Tsirelson, 1996; Gatti, Bianchi, Destro & Merati, 1992) and in fact refer to the mean thermal nuclear distribution. In this situation, the only way to evaluate indirectly to what extent quantitative values of topological characteristics depend on the atomic thermal motion effects may be a comparative topological analysis of theoretical and experimental charge densities simultaneously. Previously, such studies of L-alanine (Gatti, Bianchi, Destro & Merati, 1992) and urea (Tsirelson, 1996, and references therein) crystals have revealed quantitative, within 5%, and semiquantitative, within 10–20% (or even qualitative, within 60%), agreement between theoretically and experimentally evaluated values of ρ and $\nabla^2\rho$, respectively, at the bond critical points (saddle points of ρ between bonded atoms) between nonhydrogen atoms. The worst agreement was found between experimental and theoretical values of these properties for C—N and N—O interactions in lithium bis(tetramethylammonium) hexanitrocobaltate(III) (Bianchi, Gatti, Adovasio & Nardelli, 1996). The highest disagreement in all these studies took place for the properties of ρ at the bond critical points between atoms displaying shared (covalent) interactions. The reason for this is clear after taking into account that such interactions are worst described by the rigid-atom models usually used for X-ray diffraction refinement and that model experimental charge density appears to be mostly affected by the thermal atomic motion. On the other hand, both experimental and theoretical studies of such relatively complex crystals as L-alanine, lithium bis(tetramethylammonium) hexanitrocobaltate(III) and urea are complicated by various factors, additional to the thermal-motion effects [*e.g.* extinction, light atoms (H, Li), relatively large number of variable parameters and correlation between them, electronic correlation and basis-set effects]. That is why

† Address for correspondence: Physics Department, Mendeleev University of Chemical Technology, Miusskaya Square 8, Moscow 125047, Russia.

ISSN 0108-7673

we believe that the best test objects for application of the topological approach to experimental charge density and comparison of the results with those for theoretical ρ should be simple well studied covalent crystals, such as diamond, silicon and germanium.

Diamond, silicon and germanium crystals occupy a unique place in solid-state physics and chemistry. Much research dealing with the theoretical and experimental study of the charge density in these crystals has been published (*e.g.* Pietsch, Tsirelson & Ozerov, 1986; Spackman, 1986, 1991; Brown & Spackman, 1990, and references therein; Lu, Zunger & Deutsch, 1993, 1995, and references therein; Zou & Bader, 1995; Sakata & Sato, 1990; Takata & Sakata, 1996); however, there has been only one study (Zou & Bader, 1995) devoted to topological analysis of the (theoretical) charge density in diamond and silicon. One of the most exciting results of this study was the observation of a non-nuclear attractor in the gradient vector field of ρ observed as a low maximum in the charge density between neighboring Si atoms, only 0.009 e Å^{-3} higher than ρ at the neighboring bond critical points. According to recent reports, the previous experimental observation of non-nuclear attractors in the experimental charge density of Si (Sakata & Sato, 1990) appears to be strongly affected by the use of incomplete structure-factor sets for maximum-entropy refinement (Takata & Sakata, 1996) and by choice of prior electron density (de Vries, Briels & Feil, 1996).

In the present work, the topological approach is applied to the multipole charge densities in diamond, silicon and germanium crystals, fitted to the same sets of high-precision dynamic experimental and static theoretical structure factors. Besides topological study of the chemical bond itself in these crystals and comparison with the previous result (Zou & Bader, 1995), this allows indirect evaluation of the extent of the thermal atomic motion effect on the experimental topological characteristics in compounds with shared interatomic interactions.

2. Pseudoatom formalism

The sets of highly accurate observed structure factors used here are the same as those used in recent extensive studies of charge density in these crystals (Lu, Zunger & Deutsch, 1993, 1995, and references therein). As in the most recent study (Lu, Zunger & Deutsch, 1995), we have transformed the 'best estimate' experimental Ge static structure factors (Dewey *et al.*, 1994) to their dynamic equivalents by introducing back the correspondent Debye–Waller factor and augmenting them with the 'forbidden' F_{222} reflection (Matsushita & Kohra, 1974; Roberto, Batterman & Keating, 1974). That is, sets of 10, 18 and 13 observed dynamic structure factors for diamond, silicon and germanium crystals were used in the present study. The maximum $\sin\theta/\lambda$ values were 0.79, 1.04 and 1.07 Å^{-1}, respectively. All these data are considered to be extinction free and corrected to the anomalous-scattering contribution. The corresponding set of accurate structure factors calculated by the local density approximation, LDA (Lu, Zunger & Deutsch, 1993, and references therein), were also used for theoretical charge-density analysis.

The fitting of the multipole charge-density model to observed and theoretical structure factors has been carried out differently to previous works (Lu, Zunger & Deutsch, 1993, 1995). The following considerations were taken into account: (i) The number of structure factors is limited and the use of a large number of variable parameters is therefore not statistically justified. (ii) There is no evidence that including separate temperature factors for core and valence shells in the multipole model leads to physically meaningful results, even if such nonadiabaticity takes place. Even the standard form of the multipole model has some artificial elements, such as the description of the two-center interaction by the combination of one-center functions. In this situation, the introduction of an additional variable parameter that highly correlates with those already existing may be viewed, in some sense, as an artificial fitting procedure.

We have used the Hansen & Coppens (1978) multipole formalism for structure-factor fitting, as incorporated in the program *MOLLY*. Within this approach, the crystal electron density is described as

$$\rho(\mathbf{r}) = \sum_k \rho_k(\mathbf{r} - \mathbf{r}_k - \mathbf{u}) * t_k(\mathbf{u}), \qquad (1)$$

where ρ_k is the charge density of the kth aspherical pseudoatom and t_k is its thermal-displacement distribution. The atomic static charge density ρ_k is modeled by a multipole expansion about free atoms:

$$\rho_k(\mathbf{r}) = P_c\rho_c(r) + P_v(r)k^3\rho_v(r) + \sum_{l=1}^{4} k'^3 R_l(k'r) \sum_{m=-l}^{l} P_{lm} y_{lm}(\mathbf{r}/r), \qquad (2)$$

where ρ_c and ρ_v are spherically averaged free-atom Hartree–Fock (HF) core and valence densities normalized to one electron; y_{lm} are real spherical harmonic angular functions; R_l are normalized Slater-type radial functions

$$R_l(r) = [(\alpha_l^{n_l+3})/(n_l+2)!]r^{n_l}\exp(-\alpha_l r); \qquad (3)$$

k and k' are dimensionless expansion/contraction parameters, which can be refined in the fitting procedure along with the populations P_v and P_{lm}. The core population P_c is fixed at the appropriate value. Only octapole P_{3-2} and hexadecapole P_{40} ($P_{44} = 0.74045P_{40}$) multipole parameters are symmetry-allowed in a diamond structure (Kurki-Suonio, 1977). The initial values of exponential coefficients α_l were taken either from optimized Slater-type exponents (Clementi & Raimondi, 1963) or from previously fitted values (Lu, Zunger & Deutsch, 1993,

Table 1. *Parameters of the multipole model of diamond charge density obtained by fitting to the experimental and theoretical structure factors (see text)*

Fitted data, model	k	ξ^* (a.u.$^{-1}$)	n_3	P_{3-2}	n_4	P_{40}	B (Å^2)	R† (%)	wR† (%)
Experimental, model *A*‡§	1.00¶	3.52 (25)	4	0.327 (46)	4	0¶	0.139 (7)	0.80	0.91
Theory, model *A*§	0.997	3.531	4	0.343	4	0¶	0¶	0.77	0.98
Theory, model *B***	0.968	2.679	3	0.364	4	−0.146	0.1379¶	0.64	0.64

* $\xi = k'\alpha$. † $R = \sum|F - F_m|/\sum F$; $wR = [\sum w(F - F_m)^2/\sum wF^2]^{1/2}$, where F and F_m are moduli of observed or theoretical and model structure factors, respectively. ‡ The s^2p^2 spherical valence density configuration is used. § The multipole model is fitted to the 10 structure factors ($\sin\theta/\lambda \le 0.79$Å^{-1}). ¶ The value was fixed during the fit. ** The prepared sp^3 spherical valence density configuration is used. The multipole model is fitted to the 27 dynamic structure factors ($\sin\theta/\lambda \le 1.28$Å^{-1}) calculated by the local density approximation (Lu, Zunger & Deutsch, 1993, and references therein).

1995) and were refined with constraint $\alpha_3 = \alpha_4 (= \alpha)$. Different radial functions (sets of $n_3 \ge 3$, $n_4 \ge 4$ and spherical valence configurations) were tried in seeking to minimize the residual densities in the internuclear regions

$$\Delta\rho(\mathbf{r}) = V^{-1}\sum_{\mathbf{h}}[F(\mathbf{h}) - F_m(\mathbf{h})]\exp(-2\pi i\mathbf{h}\cdot\mathbf{r}), \quad (4)$$

where F and F_m are moduli of observed or theoretical and model structure factors, respectively, and V is the volume of the unit cell. The following spherical valence configurations were tested for $\rho_v(\mathbf{r})$ calculation from $3P$ ground-state wavefunctions (Clementi & Roetti, 1974): a ground state s^2p^2 configuration (model *A*) and a prepared sp^3 configuration (model *B*). The latter model artificially reflects the electron promotion preceding sp^3 atomic hybridization in these semiconductors and was tested previously (Hansen & Coppens, 1978) for the multipole refinement of Si. Since there are no tabulations of orbital-by-orbital (or core and valence) relativistic densities for Ge, relativistic effects were not taken into consideration in the present study. Variable parameters were fitted using a least-squares minimizing function $\sum w(F - F_m)^2$, where $w = 1/\sigma^2(F)$ or 1 for observed and theoretical structure factors, respectively. Multipole population parameters that appeared to be small and insignificant (less than 2σ) during fitting to experimental data were fixed at zero. The only exception was an experimental model charge density of Ge, where the hexadecapole term was not fixed at zero in order to reserve the flexibility of the model. The atomic thermal displacements in dynamic charge density models were considered to be harmonic. The resulting number of structure factors per variable parameter was not less than 3 for all crystals studied, except for Ge where it was 2.6.

The best-fit multipole models of both experimental and theoretical charge densities were used for topological analysis of the crystals. A critical point search, analysis and calculation of the $\nabla^2\rho(\mathbf{r})$ distribution were performed using the program *LSPROP* (Howard & Mallinson, 1992). Within this program, only covariance-matrix elements linking population parameters are used for the calculation of variance in the charge-density property.

3. Results and discussion

3.1. *Diamond*

The model parameters and disagreement factors obtained by the best fit to the experimental and theoretical structure factors of a diamond crystal are presented in Table 1. Two theoretical data sets calculated by Lu, Zunger & Deutsch (1993) were independently fitted: the same set of static structure factors as in the experiment and 27 dynamic structure factors with maximum $\sin\theta/\lambda$ value 1.28 Å^{-1}. In the latter case, the thermal-motion effect was simply introduced in the static structure factors by the Debye–Waller factor ($B = 0.1379$ Å^2). It can be seen from Table 1 that experimental and theoretical charge-density models fitted to ten structure factors using an s^2p^2 spherical valence configuration are very close to each other, displaying unnoticeable expansion/contraction of the atomic valence shell and insignificance of the hexadecapole term. This is in good agreement with previous results (Spackman, 1991; Lu, Zunger & Deutsch, 1993). On the other hand, all multipole parameters are noticeable for fitting to the theoretical dynamic structure factors when the use of the sp^3 valence configuration gives the best agreement (Table 1).

The calculated model maps of the static experimental and theoretical valence densities in the (110) plane of diamond are presented in Fig. 1. It can be seen from Fig. 1 that the fitting to the theoretical and experimental structure factors results in very similar charge distributions. The model theoretical valence density (Fig. 1*b*) is very close to the corresponding calculated density (Lu, Zunger & Deutsch, 1993) in the internuclear region. The good quality of the fitting to both experimental and theoretical structure factors is reflected by the low values of residual densities in the bonding regions (Fig. 2).

The types and properties of the critical points of the model experimental and theoretical charge densities of diamond crystal are presented in Fig. 3 and Table 2. At such points, the type and location of which are defined by the charge-density topology (Bader, 1990), the gradient of the electron density vanishes. The topology of the charge density appeared to be identical for both model experimental and theoretical charge densities and

similar to that obtained earlier for a diamond crystal from a theoretical electron-density study (Zou & Bader, 1995). The local maxima of the electron density at the nuclear positions are $(3,-3)$ critical points. In a diamond crystal, every such point is linked to four nearest-neighbor $(3,-3)$ critical points by bond paths, *i.e.* lines of maximum charge density between bonding atoms, yielding a tetrahedral molecular graph (network of bond paths). The saddle points of the charge density at the middle of each bond path are $(3,-1)$ bond critical points, which define the existence of a chemical bond between neighboring atoms in the crystal. The $(3,+3)$ cage critical points reflect a minimum of charge density at the center of the volume delimited by neighboring tetrahedral graphs. The $(3,+1)$ ring critical points are located at the charge density local minimum at the centers of rectangular planes defined by pairs of second-nearest-neighbor atoms.

The quantitative agreement takes place between experimental and theoretical (model *A*) values of the properties of the charge density of the diamond crystal (Table 2). On the other hand, these values display a quantitative and semiquantitative agreement with the ρ and $\nabla^2\rho$ values, respectively, at the critical points of the model *B* theoretical charge density (Table 2). In contrast to this, the value of the diamond Hartree–Fock charge density (Zou & Bader, 1995) at the bond critical point is noticeably higher than the corresponding experimental values (Table 2) and that calculated by the local density approximation (Lu, Zunger & Deutsch, 1993). The disagreement between values of $\nabla^2\rho$ at these points is consequently much higher.

In order to understand the main factors affecting the results of the topological study, the variation of the properties of the model (*A* and *B*) theoretical charge density at the bond critical points with the number of

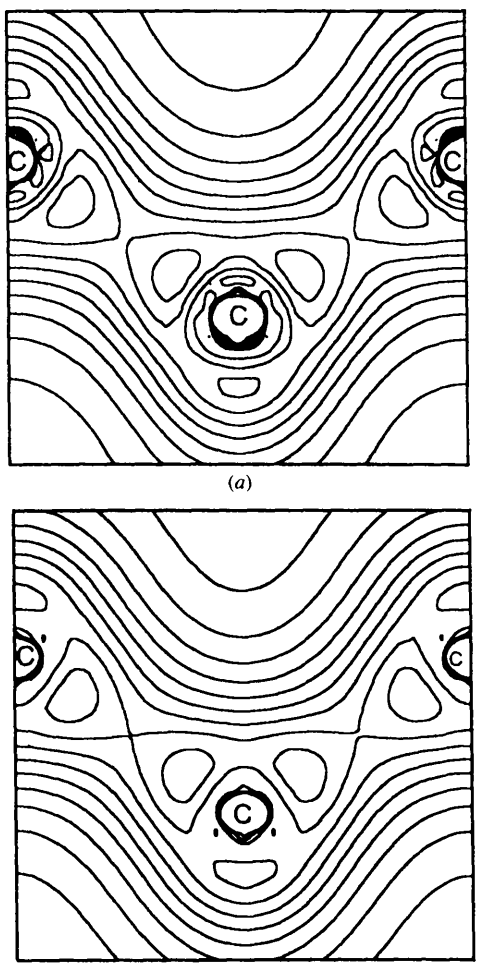

(*a*)

(*b*)

Fig. 1. Static valence-charge densities in the (110) plane of a diamond crystal calculated from multipole models fitted to (*a*) experimental and (*b*) theoretical (model *B*) structure factors. Contour intervals are 0.2 e Å^{-3}.

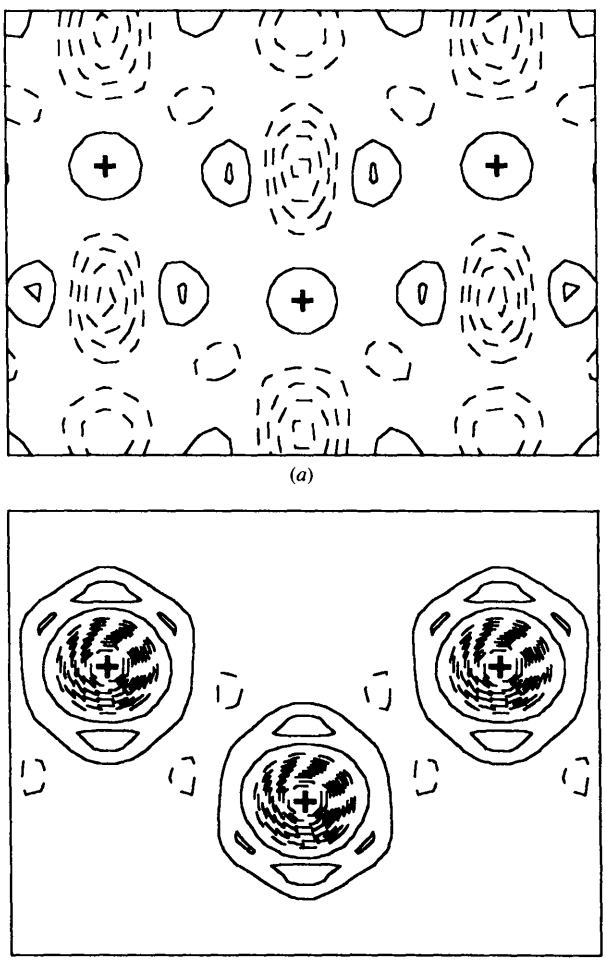

(*a*)

(*b*)

Fig. 2. Residual densities in the (110) plane of a diamond crystal calculated from multipole models fitted to (*a*) experimental and (*b*) theoretical (model *B*) structure factors. Contour intervals are 0.02 e Å^{-3}.

Table 2. *Properties of the static model charge density at the bond (3, −1), cage (3, +3) and ring (3, +1) critical points of the diamond crystal*

Subscripts b, c and r denote bond, cage and ring critical points, respectively. $\lambda_1 = \lambda_2$ and λ_3 are curvatures of ρ at the bond critical point perpendicular and parallel to the bond path, respectively.

Properties	Experimental, model *A*	Theory, model *A*	Theory, model *B*
ρ_b* (e Å^{-3})	1.596 (45)	1.620	1.603
$\nabla^2\rho_b$ (e Å^{-5})	−10.16 (8)	−10.92	−12.26
$\lambda_1 = \lambda_2$, λ_3	−10.10, 10.04	−10.37, 9.82	−10.24, 8.22
ρ_c (e Å^{-3})	0.101 (5)	0.100	0.093
$\nabla^2\rho_c$ (e Å^{-5})	1.57 (5)	1.55	1.77
ρ_r (e Å^{-3})	0.160 (9)	0.160	0.138
$\nabla^2\rho_r$ (e Å^{-5})	2.14 (9)	2.12	2.65

* The *ab initio* calculated value of ρ_b is 1.59 e Å^{-3} (Lu, Zunger & Deutsch, 1993).

Table 3. *The variation of the properties of charge density at critical points and of disagreement factor R of the fitted diamond crystal models with the maximum $\sin\theta/\lambda$ value (Å^{-1}) of structure factors included in the fit*

The *A* and *B* models are fitted to the various sets of the calculated dynamic structure factors (Lu, Zunger & Deutsch, 1993, and references therein). The multipole expansion of the charge density up to the hexadecapole term (four variable parameters; $n_3 = 3$, $n_4 = 4$) is applied for both models.

	$(\sin\theta/\lambda)_{max} = 0.79$ $N^* = 10$		$(\sin\theta/\lambda)_{max} = 0.94$ $N = 13$		$(\sin\theta/\lambda)_{max} = 1.00$ $N = 16$		$(\sin\theta/\lambda)_{max} = 1.19$ $N = 23$		$(\sin\theta/\lambda)_{max} = 1.28$ $N = 27$	
Properties	Model *A*	Model *B*	Model *A*	Model *B*	Model *A*	Model *B*	Model *A*	Model *B*	Model *A*	Model *B*
ρ_b (e Å^{-3})	1.58	1.61	1.58	1.61	1.57	1.60	1.57	1.60	1.57	1.60
$\nabla^2\rho_b$ (e Å^{-5})	−9.46	−12.44	−9.27	−12.39	−9.04	−12.32	−8.84	−12.27	−8.80	−12.26
ρ_c (e Å^{-3})	0.101	0.091	0.103	0.092	0.103	0.092	0.107	0.093	0.107	0.093
$\nabla^2\rho_c$ (e Å^{-5})	1.66	1.79	1.65	1.78	1.64	1.78	1.62	1.77	1.62	1.77
ρ_r (e Å^{-3})	0.148	0.136	0.149	0.137	0.150	0.137	0.153	0.138	0.152	0.138
$\nabla^2\rho_r$ (e Å^{-5})	2.38	2.68	2.36	2.67	2.34	2.66	2.30	2.65	2.30	2.65
R (%)	0.31	0.45	0.55	0.52	0.77	0.57	1.19	0.62	1.33	0.64

* Number of structure factors included in the fit.

theoretical dynamic structure factors included in the fit was studied (Table 3). In all cases, the four variable parameters, k, k', P_{3-2} and P_{40}, were refined. It could be seen (Table 3) that the correct choice between the *A* or *B* flexible multipole model of the crystal charge density strongly depends on the number of the structure factors per variable parameter, which should be not less than 3. On the other hand, the convergence of the properties of each fitted model density (*A* and *B*) at the critical points with the maximum $\sin\theta/\lambda$ value of the structure factors included in the fit is quite fast (Table 3). This reflects the fact that the high-order structure factors are mostly important for the proper description of the regions with the rapidly varying charge density and its Laplacian, *i.e.* core regions, while for our task only the valence region is of main interest. It can also be seen (Tables 2 and 3) that inclusion of the hexadecapole term in model *A* does not lead to considerable variations of the calculated properties.

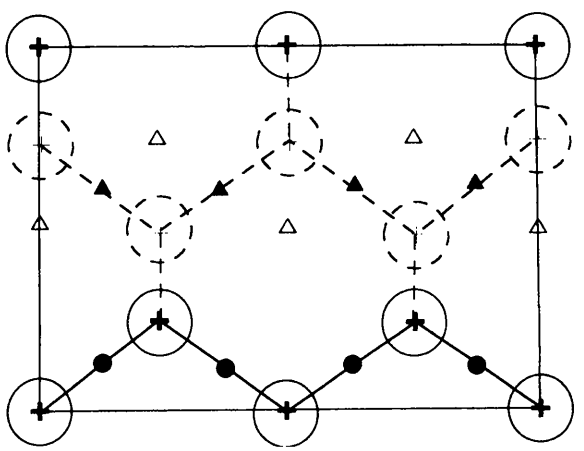

Fig. 3. Location of the critical points in the (110) plane of the diamond crystal unit cell. The bond, cage and ring critical points are denoted by dots, open and full triangles, respectively. The projections of the out-of-plane atoms and bond lines are shown by dashes.

Maps of the Laplacian of the experimental and theoretical model static ρ distribution in the (110) plane of the diamond crystal are presented in Fig. 4. In both maps, the bridges of the negative Laplacian of ρ connect planar chains of C atoms throughout the crystal.

3.2. *Silicon*

The model parameters and disagreement factors obtained by best fitting to the experimental and theoretical structure factors of a silicon crystal are presented in Table 4. Two fitted multipole models, *A* and *B*, gave almost the same agreement with the experimental structure factors. The high correlation (with maximum

Table 4. *Parameters of the multipole model of silicon charge density obtained by fitting to the experimental and theoretical structure factors (see text)*

Fitted data, model	k	ξ (a.u.$^{-1}$)	n_3	P_{3-2}	n_4	P_{40}	B (Å^2)	R (%)	wR (%)
Experimental, model A*†	0.958 (10)	2.41 (8)	4	0.408 (32)	4	−0.099 (20)	0.464 (1)	0.16	0.18
Experimental, model B*†	0.996 (13)	2.34 (5)	4	0.440 (38)	4	−0.116 (23)	0.468 (2)	0.17	0.19
Theory, model B†	1.015	2.36‡	4	0.400	4	−0.086	0‡	0.26	0.29

* The maximum correlation coefficient 0.997 is observed between k' and P_{3-2} parameters. † The multipole model is fitted to the 18 structure factors (sin $\theta/\lambda \leq 1.04$ Å^{-1}). ‡ The value was fixed during the fit.

correlation coefficient 0.997) was observed between k' and P_{3-2} parameters during fitting of both models. The noticeable expansion of the atomic s^2p^2 valence shell is found in accordance with results of previous studies (Hansen & Coppens, 1978; Spackman, 1986; Lu, Zunger & Deutsch, 1993). The best fitting to the theoretical structure factors was performed by the multipole model B (Table 4). In order to obtain a stable convergence of the parameters, the k' parameter was fixed at the mean value on the last steps of refinement of this model. It should be noted that the obtained multipole parameters of model B of the experimental and theoretical charge densities almost agree with each other within calculated e.s.d.'s.

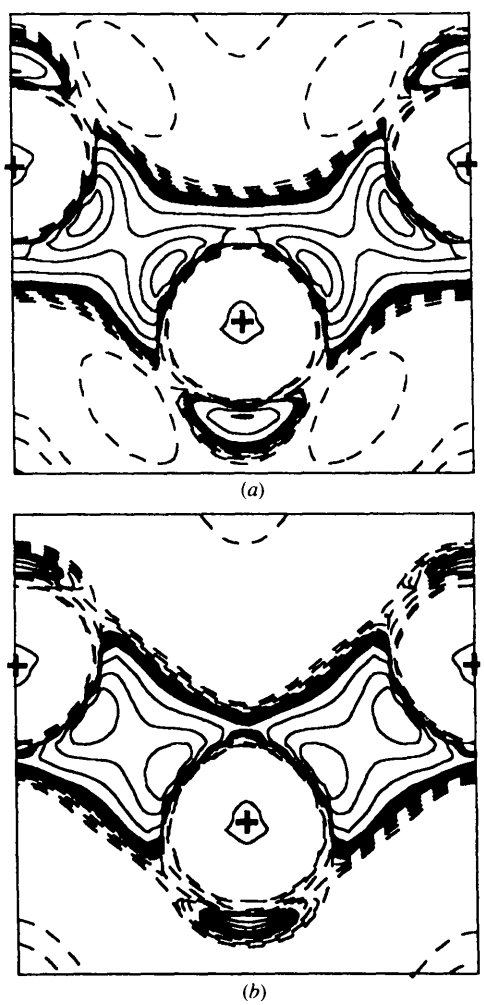

Fig. 4. $-\nabla^2\rho$ maps in the (110) plane of a diamond crystal calculated from multipole models fitted to (*a*) experimental and (*b*) theoretical (model B) structure factors. Contour values are ±0.05, ±0.10, ±0.15, ±0.20 e Å^{-5} increasing in powers of 10 to ±20.00 e Å^{-5}. Positive and negative contours are represented by solid and dashed lines. Some contours overlap with one another when $-\nabla^2\rho$ undergoes a change in sign. The maximum contours along bond paths are (*a*) 20.00 and (*b*) 15.00 e Å^{-5}.

The calculated model maps of the static experimental and theoretical valence densities in the (110) plane of silicon are presented in Fig. 5. The model experimental valence density (Fig. 5*a*) is close to the previously calculated pseudoatom densities (Spackman, 1986; Lu, Zunger & Deutsch, 1993), while the model theoretical valence density (Fig. 5*b*) is similar to the corresponding calculated density (Lu, Zunger & Deutsch, 1993) in the internuclear region. It can be seen from Fig. 5 that, in spite of the overall agreement between experimental and theoretical static valence density maps, there is still some difference in the width of the twin bonding peak between neighboring atoms. The low values of residual densities in the bonding regions (Fig. 6) reflect a good quality of the fitting to both experimental and theoretical structure factors.

The set of critical points of both experimental and theoretical model charge densities of silicon (Table 5) appeared to be the same as in a diamond crystal (Fig. 3). Thus, contrary to the results of the HF study of the topology of charge density in a silicon crystal (Zou & Bader, 1995) and to the results of the maximum-entropy refinement (Sakata & Sato, 1990; Takata & Sakata, 1996) of accurate X-ray data, we have not found within achieved accuracy non-nuclear attractors, *i.e.* (3, −3) critical points, between neighboring Si atoms in the model charge densities derived from both the experimental and theoretical (Lu, Zunger & Deutsch, 1993) structure-factor data. The absence of such attractors in the LDA silicon density (Lu, Zunger & Deutsch, 1993) is quite evident from the published calculated ρ_{val} distribution along the Si—Si bond. The possible reason for such a discrepancy might be the insufficient accuracy in the HF results (Zou & Bader, 1995) and the maximum-entropy refinement being noticeably affected both by the use of an incomplete structure-factor data set (Takata & Sakata, 1996) and by the choice of prior electron density

Table 5. *Properties of the static model charge density at the bond, cage and ring critical points of the silicon crystal*

Properties	Experimental, model *A*	Experimental, model *B*	Theory, model *B*
ρ_b* (e Å^{-3})	0.582 (1)	0.582 (1)	0.561
$\nabla^2\rho_b$ (e Å^{-5})	−2.92 (1)	−3.07 (1)	−2.63
$\lambda_1 = \lambda_2$, λ_3	−1.85, 0.78	−1.83, 0.60	−1.72, 0.82
ρ_c (e Å^{-3})	0.027 (1)	0.026 (1)	0.025
$\nabla^2\rho_c$ (e Å^{-5})	0.19 (1)	0.20 (1)	0.20
ρ_r (e Å^{-3})	0.041 (1)	0.040 (1)	0.040
$\nabla^2\rho_r$ (e Å^{-5})	0.29 (1)	0.30 (1)	0.30

* The *ab initio* calculated value of ρ_b is 0.56 e Å^{-3} (Lu, Zunger & Deutsch, 1993).

(de Vries, Briels, & Feil, 1996). The absolute value of the silicon HF charge density (Zou & Bader, 1995) at the bond critical points $\rho_b = 0.622$ e Å^{-3} and at the non-nuclear attractor $\rho_n = 0.631$ e Å^{-3} are noticeably higher than the experimental and theoretical model ρ_b values (Table 5) and the value, $\rho_b = 0.56$ e Å^{-3}, calculated by the local density approximation (Lu, Zunger & Deutsch, 1993).

The quantitative and semiquantitative agreement takes place between experimental and theoretical (local density approximation) values of the ρ and $\nabla^2\rho$, respectively, at the critical points of silicon model charge densities (Table 5). It should be noted that the obtained agreement is model (*A* or *B*) independent.

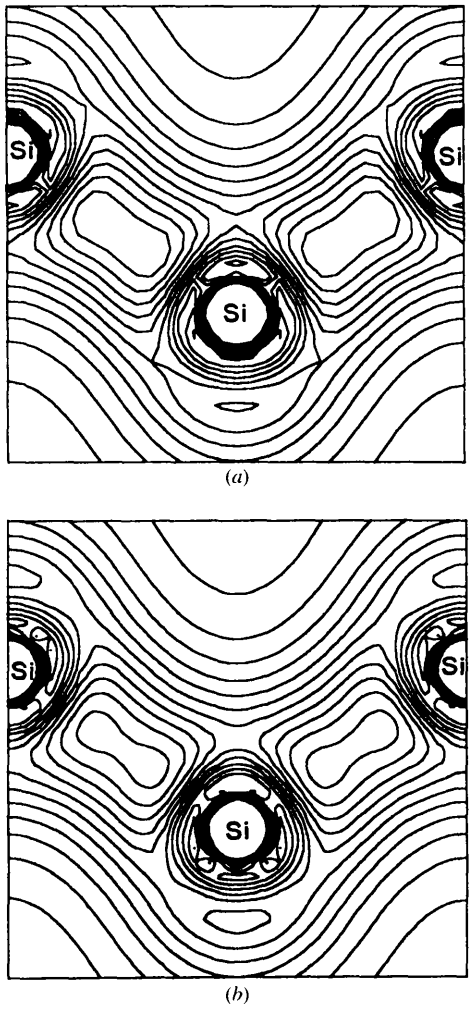

Fig. 5. Static valence-charge densities in the (110) plane of a silicon crystal calculated from multipole models fitted to (*a*) experimental (model *A*) and (*b*) theoretical structure factors. Contour intervals are 0.05 e Å^{-3}.

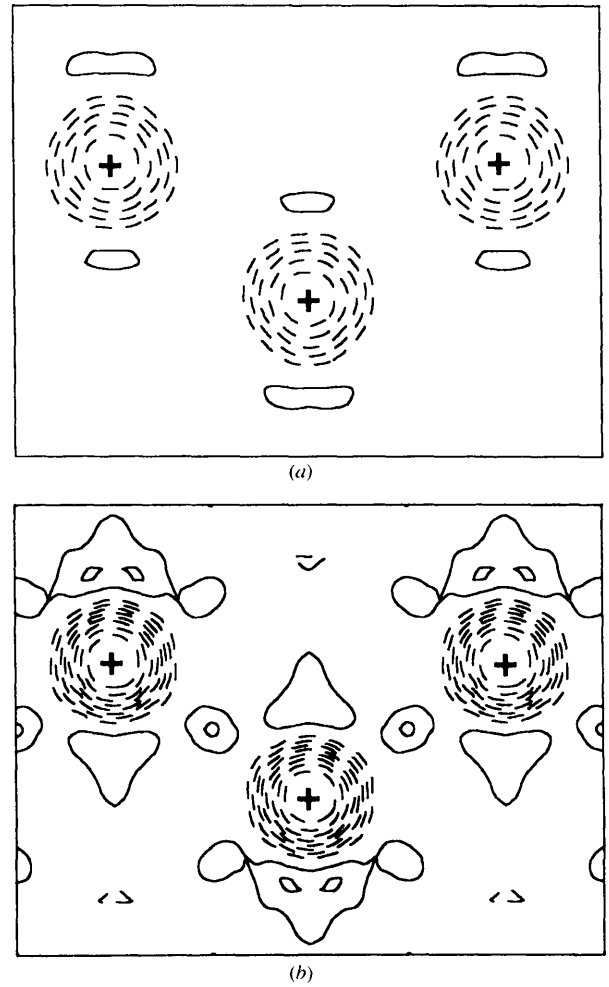

Fig. 6. Residual densities in the (110) plane of a silicon crystal calculated from multipole models fitted to (*a*) experimental (model *A*) and (*b*) theoretical structure factors. Contour intervals are 0.01 e Å^{-3}.

Table 6. *The influence of the variation of the orbital exponent ξ on the experimental topological characteristics of the silicon crystal, model A; the ξ variation is applied within the unchanged values of the R and wR (Table 4)*

Properties	$\xi = 2.40$	$\xi = 2.42$	$\xi = 2.44$	$\xi = 2.44$
ρ_b (e Å^{-3})	0.579	0.578	0.577	0.576
$\nabla^2\rho_b$ (e Å^{-5})	−2.89	−2.86	−2.84	−2.82
$\lambda_1 = \lambda_2$, λ_3	−1.83, 0.76	−1.83, 0.80	−1.84, 0.58	−1.84, 0.87
ρ_c (e Å^{-3})	0.027	0.027	0.028	0.029
$\nabla^2\rho_c$ (e Å^{-5})	0.19	0.19	0.19	0.19
ρ_r (e Å^{-3})	0.040	0.041	0.042	0.042
$\nabla^2\rho_r$ (e Å^{-5})	0.30	0.29	0.29	0.29

For a further test of the stability of the obtained results, the influence of the variation of the orbital exponent ξ, within unchanged R and wR factors, on the topological characteristics of the model experimental charge density of silicon was studied (Table 6). As mentioned above, the ξ value is highly correlated through the k' parameter with the P_{3-2} term during fitting to the experimental structure factors. It can be seen from Table 6 that the ξ variations within the same values of the disagreement factors do not spoil the observed quantitative and semiquantitative agreement with the critical point properties of the model theoretical charge density.

Since covariance-matrix elements linking k, k' and B parameters are not used for the calculation of variance in the charge-density property by the *LSPROP* (Howard & Mallinson, 1992) program, the obtained e.s.d. values (Table 6) should be considered as underestimated. This is why we additionally tested the variation of the calculated properties by monotonously varying all the multipole parameters (model A) fitted to the experimental structure factors within $\pm 1\sigma$. This resulted in the maximum variation of the $\nabla^2\rho_b$ value of 12% yielding a maximum disagreement of 24% with the corresponding value of the theoretical model charge density.

Maps of the Laplacian of the experimental and theoretical model static ρ distribution in the (110) plane of the silicon crystal are presented in Fig. 7. The two maps are very close to each other, displaying large regions of negative Laplacian of ρ between neighboring atoms.

3.3. *Germanium*

The best fit to both the experimental and theoretical structure factors of the germanium crystal was obtained within model A. The high correlation (maximum correlation coefficient is 0.997) was observed between k' and P_{3-2} parameters during fitting of the experimental density model. In order to remove completely this correlation, the orbital exponent α was fixed and its step-by-step variation within an unchanged wR value was performed searching for the minimum residual density in the internuclear region. The resulting model parameters and disagreement factors are presented in Table 7. The value of the orbital exponent α obtained and the noticeable expansion of the atomic valence shell discovered in the experimental model (Table 7) are in good agreement with the results of Lu, Zunger & Deutsch (1995).

The model maps of the static experimental and theoretical valence densities in the (110) plane of germanium are presented in Fig. 8. The two maps display a noticeable difference, while the model theoretical valence density (Fig. 8*b*) is in general agreement with the

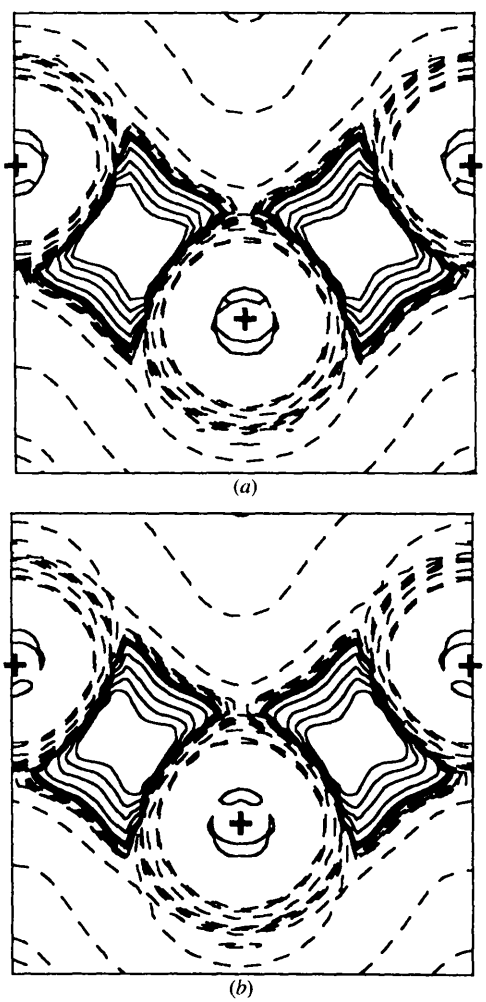

Fig. 7. $-\nabla^2\rho$ maps in the (110) plane of a silicon crystal calculated from multipole models fitted to (*a*) experimental (model *A*) and (*b*) theoretical structure factors. Contour values are as for Fig. 4. The maximum contours along bond paths are 2.00 e Å^{-5}.

Table 7. *Parameters of the multipole model of germanium charge density obtained by fitting to the experimental and theoretical structure factors (see text)*

Fitted data, model	k	ξ (a.u.$^{-1}$)	n_3	P_{3-2}	n_4	P_{40}	B (Å^2)	R (%)	wR (%)
Experimental, model *A**	0.918 (2)	2.10†	4	0.386 (6)	4	−0.103 (203)	0.552 (4)	0.38	0.31
Theory, model *A**	0.957	2.736	6	0.307	6	−0.161	0†	0.28	0.29

* The multipole model is fitted to the 13 static structure factors ($\sin\theta/\lambda \leq 1.07$ Å^{-1}). † The value was fixed during the fit.

calculated LDA valence density (Lu, Zunger & Deutsch, 1993). The quality of fit of both experimental and theoretical models is presented by the residual densities in Fig. 9. It is seen that the fitting to the observed structure factors is noticeably worse. A possible reason for this is the lowest quality of the observed structure factors for this crystal in comparison to diamond and especially silicon crystals.

The set of critical points of both experimental and theoretical model static charge densities of the germanium crystal (Table 8) is the same as in the diamond and silicon crystals (Fig. 3). The quantitative agreement takes place between model experimental and theoretical values of ρ_b, ρ_c and $\nabla^2\rho_b$ (Table 8). At the same time, for the ρ_r, $\nabla^2\rho_r$ and $\nabla^2\rho_c$ values such agreement is semiquantitative.

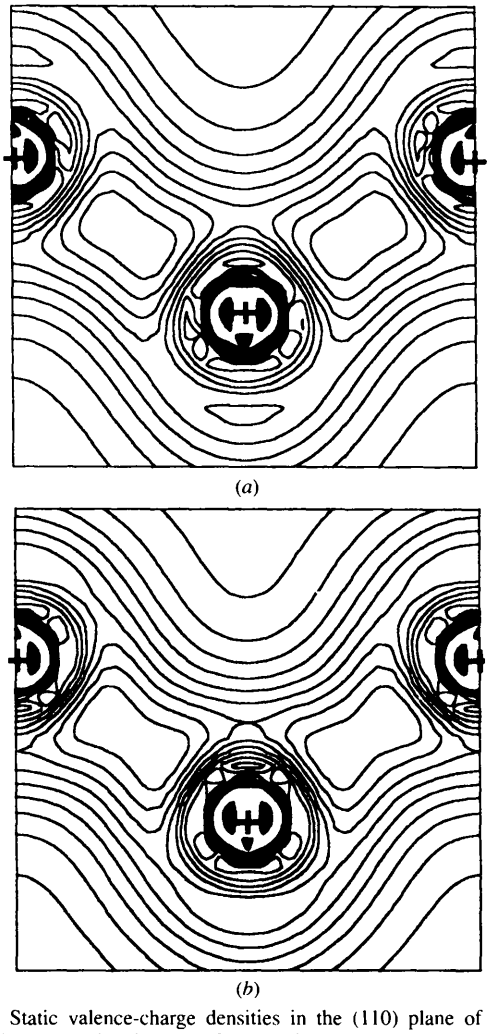

Fig. 8. Static valence-charge densities in the (110) plane of a germanium crystal calculated from multipole models fitted to (*a*) experimental and (*b*) theoretical structure factors. Contour intervals are 0.05 e Å^{-3}.

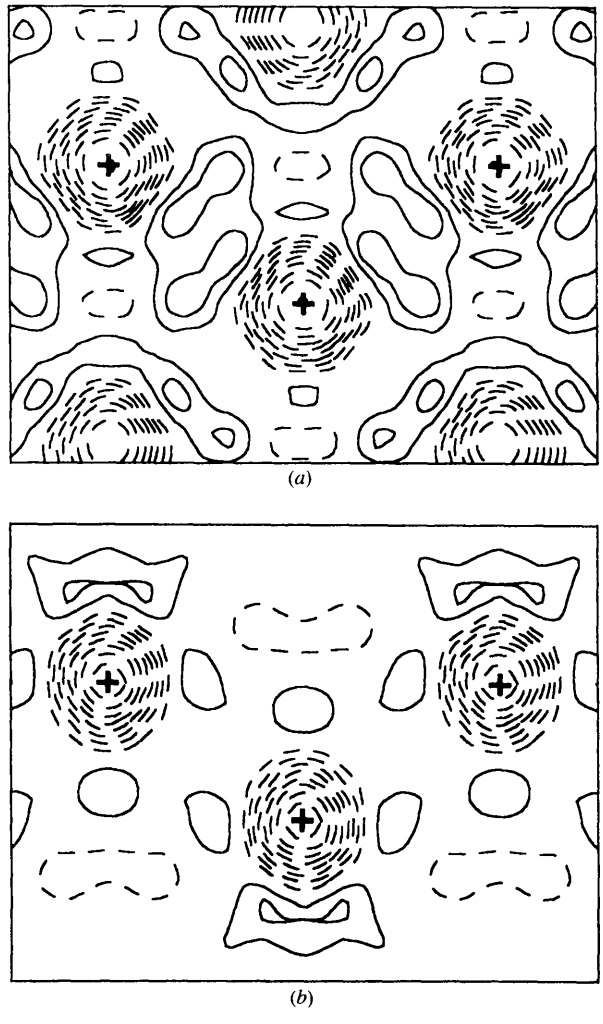

Fig. 9. Residual densities in the (110) plane of a germanium crystal calculated from multipole models fitted to (*a*) experimental and (*b*) theoretical structure factors. Contour intervals are 0.02 e Å^{-3}.

Table 8. *Properties of the static model charge density at the bond, cage and ring critical points of the germanium crystal*

Properties	Experimental, model *A*	Theory, model *A*
ρ_b* (e Å^{-3})	0.502 (1)	0.503
$\nabla^2\rho_b$ (e Å^{-5})	−1.18 (1)	−1.18
$\lambda_1 = \lambda_2$, λ_3	−1.37, 1.56	−1.43, 1.68
ρ_c (e Å^{-3})	0.021 (1)	0.022
$\nabla^2\rho_c$ (e Å^{-5})	0.19 (1)	0.148
ρ_r (e Å^{-3})	0.035 (1)	0.029
$\nabla^2\rho_r$ (e Å^{-5})	0.29 (1)	0.253

* The *ab initio* calculated value of ρ_b is 0.49 e Å^{-3} (Lu, Zunger & Deutsch, 1993).

Maps of the Laplacian of the model experimental and theoretical static ρ distribution in the (110) plane of germanium are presented in Fig. 10. The two maps are very close to each other, displaying relatively small regions of the negative Laplacian of ρ between neighboring atoms elongated perpendicular to the bond direction.

3.4. *Comparative analysis*

Properties of the charge density at the bond critical point characterize the chemical bonding between neighboring atoms (Bader, 1990; Bader & Essen, 1984). The sign of the Laplacian of ρ at this point reflects which of two competing effects is dominant: contraction of ρ perpendicular to the bond path (the corresponding curvatures λ_1 and λ_2 are negative) or the expansion of ρ parallel to this path ($\lambda_3 > 0$). The former leads to concentration of charge along the bond path, while the latter leads to its depletion and separate concentration in the basins of neighboring atoms. Thus, a higher value of the negative Laplacian of ρ at the bond critical point reflects the higher accumulation of charge in the interatomic region along the bond path and a stronger covalent interaction. The values obtained for $\nabla^2\rho$ and ρ at the bond critical points (Tables 2, 5 and 8) correspond to covalent interatomic interactions in all crystals studied. Covalent interactions are strongest in diamond and rapidly weaken in the direction of Ge.

The value of $\nabla^2\rho$ at the cage critical point reflects the resistance of the diamond-type crystal to compression (Zou & Bader, 1995). Values of $\nabla^2\rho_c$ listed in Tables 2, 5 and 8 exhibit the same trend as those of the bulk modulus B, which change dramatically from 443 GPa in diamond (Chang & Cohen, 1987) to fairly similar values of 99 GPa (Chang & Cohen, 1987) and 77 GPa (McSkimin & Andreatch, 1963, 1964) in silicon and germanium crystals, respectively.

The distributions of the Laplacian of model experimental and theoretical static charge densities (Figs. 4, 7 and 10) are close to each other in all crystals studied. It is evident from these maps that the Laplacian of charge densities along the bond paths reflects the tendencies that were discussed above on the basis of the properties of ρ at the bond critical points. The region of the negative Laplacian is contiguous over the interatomic regions of neighboring atoms in diamond and silicon crystals. This is more pronounced for the diamond crystal where bridges of negative Laplacian of ρ connect planar chains of C atoms throughout the crystal. In a germanium crystal, the region of negative $\nabla^2\rho$ is much narrower and concentrated around the bond critical-point location. According to the local virial theorem (Bader, 1990; Bader & Essen, 1984),

$$(\hbar^2/4m)\nabla^2\rho = 2G(\mathbf{r}) + V(\mathbf{r}), \qquad (5)$$

a negative sign of the Laplacian of ρ indicates that the stabilizing contribution of the negative local potential-energy density $V(\mathbf{r})$ to the virial (and to the total electronic energy) is dominant in a particular region of space,

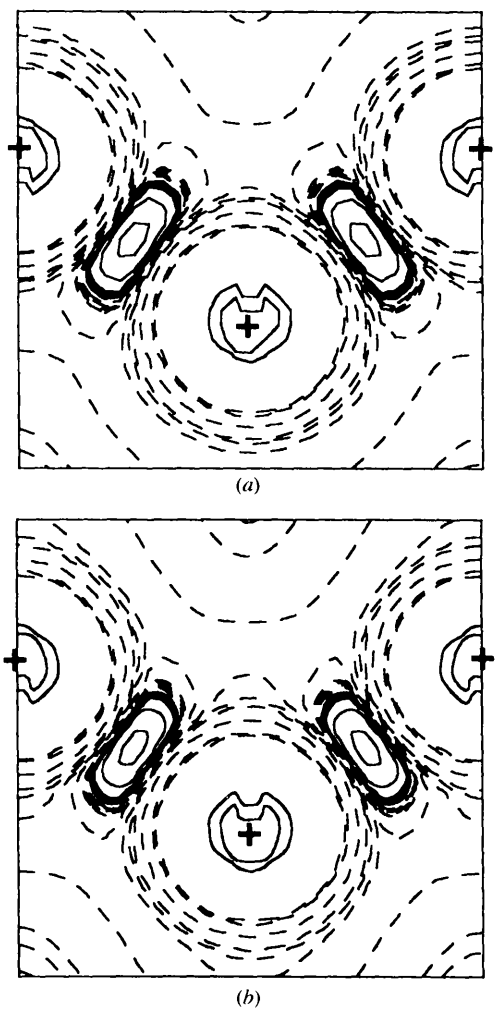

Fig. 10. $-\nabla^2\rho$ maps in the (110) plane of a germanium crystal calculated from multipole models fitted to (*a*) experimental and (*b*) theoretical structure factors. Contour values are as for Fig. 4. The maximum contours along bond paths are 1.0 e Å^{-5}.

where the electronic charge is locally concentrated. Conversely, the destabilizing contribution of the positive kinetic energy density $G(\mathbf{r})$ is dominant in the regions of space with positive values of $\nabla^2\rho$, where a local depletion of the electronic charge takes place. This consideration accounts for the stabilizing nature of the charge accumulation in the internuclear region and hence for the strong covalent interatomic bond in the diamond crystal and for decreasing covalency in the series C, Si, Ge crystals. In other words, it reflects the increasing metallic character (charge delocalization and lowering band gap) of this series of semiconductors. The increase in harmonic atomic displacements at room temperature with the increase of atomic weight (Tables 1, 4 and 7) can also be viewed as a result of significant covalent-bond weakening in this series.

4. Conclusions

The present analysis of the model charge densities of diamond, silicon and germanium crystals fitted to highly accurate published (Lu, Zunger & Deutsch, 1993, 1995) experimental and theoretical structure factors shows the following: (i) The obtained experimental and theoretical model static charge densities of both diamond and silicon crystals agree with each other and with previous results (Lu, Zunger & Deutsch, 1993, 1995). Worse agreement is observed for these charge densities in Ge crystals. (ii) Topological analysis of model experimental and model theoretical charge densities reveals an identical set of critical points of ρ in all crystals. Contrary to the previous theoretical (Zou & Bader, 1995) and experimental (Sakata & Sato, 1990; Takata & Sakata, 1996) studies, no non-nuclear attractors were found within achieved accuracy in any of the crystals studied. This means that the molecular graphs are identical in all crystals and coincide with the nuclear configuration. (iii) It is shown (Table 3) that the correct choice of flexible multipole model of the crystal charge density strongly depends on the number of structure factors per variable parameter, which should be at least not less than 3. On the other hand, the convergence of the properties of the fitted model charge density at the critical points with the maximum $\sin\theta/\lambda$ value of the structure factors included in the fit is quite fast (Table 3). (iv) Experimental and theoretical values of ρ and $\nabla^2\rho$ agree quantitatively and semiquantitatively, respectively, at the critical points of model charge densities. For the Ge crystal, such agreement is worse for the ρ value at the ring critical point. These results suggest that atomic thermal-motion effects are not crucial for a semiquantitative study of the topological characteristics of highly accurate experimental charge densities of crystals displaying shared interatomic interactions. (v) Despite the qualitative topological identity of the charge densities, a noticeable quantitative difference in the properties of ρ is found in the series C, Si, Ge. Thus, consistent with traditional considerations, the charge density at the bond critical points and the Laplacian distribution in these crystals reflects the strong covalent bond in diamond crystals, which sharply weakens on descending the series. Such behavior is consistent with the increasing metallic character and atomic displacement amplitude observed when moving from diamond to germanium crystals.

YAA is grateful to Professor V. G. Tsirelson for invaluable discussions. This study was supported by a Science and Technology Promotion Fund grant to one of the authors (FPO).

References

Bader, R. F. W. (1990). *Atoms in Molecules – a Quantum Theory*. Oxford University Press.
Bader, R. F. W. & Essen, H. (1984). *J. Chem. Phys.* **80**, 1943–1960.
Bianchi, R., Gatti, C., Adovasio, V. & Nardelli, M. (1996). *Acta Cryst.* B**52**, 471–478.
Brown, A. S. & Spackman, M. A. (1990). *Acta Cryst.* A**46**, 381–387.
Chang, K. J. & Cohen, M. L. (1987). *Phys. Rev. B*, **35**, 8196–8201.
Clementi, E. & Raimondi, D. L. (1963). *J. Chem. Phys.* **38**, 2686–2689.
Clementi, E. & Roetti, C. (1974). *At. Data Nucl. Data Tables*, **14**, 177–478.
Craven, B. M. & Stewart, R. F. (1990). *Trans. Am. Crystallogr. Assoc.* **26**, 41–54.
Destro, R. & Merati, F. (1995). *Acta Cryst.* B**51**, 559–570.
Dewey, M. S., Kessler, E. G., Greene, G. L., Deslattes, D., Sacchetti, F., Petrillo, C., Freund, A., Böner, H. G., Robinson, S. & Schillebeecks, P. (1994). *Phys. Rev. B*, **50**, 2800–2808.
Dunitz, J. D., Schweizer, W. B. & Seiler, P. (1983). *Helv. Chim. Acta*, **66**, 123–133, 134–137.
Dunitz, J. D. & Seiler, P. (1983). *J. Am. Chem. Soc.* **105**, 7056–7058.
Gatti, C., Bianchi, R., Destro, R. & Merati, F. (1992). *J. Mol. Struc. Theoret. Chem.* **255**, 409–433.
Hansen, N. K. & Coppens, P. (1978). *Acta Cryst.* A**34**, 909–921.
Hirshfeld, F. L. (1971). *Acta Cryst.* B**27**, 769–781.
Howard, S. T. & Mallinson, P. R. (1992). *LSPROP. A One-Electron Properties Package for LSMOL*. Unpublished.
Iversen, B. B., Larsen, F. K., Souhassou, M. & Takata, M. (1995). *Acta Cryst.* B**51**, 580–591.
Kapphahn, M., Tsirelson, V. G. & Ozerov, R. P. (1988). *Port. Phys.* **19**, 213–216.
Kurki-Suonio, K. (1977). *Isr. J. Chem.* **16**, 115–123.
Lu, Z. W., Zunger, A. & Deutsch, M. (1993). *Phys. Rev. B*, **47**, 9385–9410.
Lu, Z. W., Zunger, A. & Deutsch, M. (1995). *Phys. Rev. B*, **52**, 11904–11911.
McSkimin, H. J. & Andreatch, P. Jr (1963). *J. Appl. Phys.* **34**, 651–655.
McSkimin, H. J. & Andreatch, P. Jr (1964). *J. Appl. Phys.* **35**, 2161–2165.

Matsushita, T. & Kohra, K. (1974). *Phys. Status Solidi*, **24**, 531–541.
Pietsch, U., Tsirelson, V. G. & Ozerov, R. P. (1986). *Phys. Status Solidi B*, **137**, 441–447.
Roberto, J. B., Batterman, B. W. & Keating, D. T. (1974). *Phys. Rev. B*, **9**, 2590–2599.
Sakata, M. & Sato, M. (1990). *Acta Cryst.* A**46**, 263–270.
Savariault, J. M. & Lehmann, M. S. (1980). *J. Am. Chem. Soc.* **102**, 1298–1303.
Spackman, M. A. (1986). *Acta Cryst.* A**42**, 271–281.
Spackman, M. A. (1991). *Acta Cryst.* A**47**, 420–427.
Stewart, R. F. (1976). *Acta Cryst.* A**32**, 565–574.
Takata, M. & Sakata, M. (1996). *Acta Cryst.* A**52**, 287–290.
Tsirelson, V. G. (1996). *Can. J. Chem.* **74**, 1171–1179.
Tsirelson, V. G. & Ozerov, R. P. (1996). *Electron Density and Bonding in Crystals*. Bristol: IOP Publishing.
Vries, R. Y. de, Briels, W. J. & Feil, D. (1996). *Phys. Rev. Lett.* **77**, 1719–1722.
Zou, P. F. & Bader, R. F. W. (1995). *Acta Cryst.* A**50**, 714–725.